Water track distribution and effects on carbon dioxide flux in an eastern Siberian upland tundra landscape

2016 Environ. Res. Lett. 11 045002

(http://iopscience.iop.org/1748-9326/11/4/045002)

Environmental Research Letters

LETTER

Water track distribution and effects on carbon dioxide flux in an eastern Siberian upland tundra landscape

Salvatore R Curasi[1,2], **Michael M Loranty**[1] **and Susan M Natali**[3]

[1] Department of Geography, Colgate University, Hamilton, NY 13346, USA
[2] Department of Biological Sciences, University of Notre Dame, Notre Dame, IN 46556, USA
[3] Woods Hole Research Center, Falmouth, MA 02540, USA

E-mail: scurasi@nd.edu

Keywords: arctic, tundra, climate change, water track, shrub, remote sensing, carbon flux

Supplementary material for this article is available online

OPEN ACCESS

RECEIVED
7 November 2015

REVISED
5 March 2016

ACCEPTED FOR PUBLICATION
7 March 2016

PUBLISHED
7 April 2016

Abstract

Shrub expansion in tundra ecosystems may act as a positive feedback to climate warming, the strength of which depends on its spatial extent. Recent studies have shown that shrub expansion is more likely to occur in areas with high soil moisture and nutrient availability, conditions typically found in sub-surface water channels known as water tracks. Water tracks are 5–15 m wide channels of subsurface water drainage in permafrost landscapes and are characterized by deeper seasonal thaw depth, warmer soil temperatures, and higher soil moisture and nutrient content relative to adjacent tundra. Consequently, enhanced vegetation productivity, and dominance by tall deciduous shrubs, are typical in water tracks. Quantifying the distribution of water tracks may inform investigations of the extent of shrub expansion and associated impacts on tundra ecosystem carbon cycling. Here, we quantify the distribution of water tracks and their contribution to growing season CO_2 dynamics for a Siberian tundra landscape using satellite observations, meteorological data, and field measurements. We find that water tracks occupy 7.4% of the 448 km^2 study area, and account for a slightly larger proportion of growing season carbon uptake relative to surrounding tundra. For areas inside water tracks dominated by shrubs, field observations revealed higher shrub biomass and higher ecosystem respiration and gross primary productivity relative to adjacent upland tundra. Conversely, a comparison of graminoid-dominated areas in water tracks and inter-track tundra revealed that water track locations dominated by graminoids had lower shrub biomass yet increased net uptake of CO_2. Our results show water tracks are an important component of this landscape. Their distribution will influence ecosystem structural and functional responses to climate, and is therefore of importance for modeling.

1. Introduction

Climate warming is relaxing constraints on vegetation productivity in arctic tundra ecosystems imposed by low temperatures and short growing seasons (ACIA 2005, Myers-Smith *et al* 2011, IPCC 2014). Observational evidence indicates that warming and associated consequences, such as permafrost thaw, stimulate vegetation productivity (Walker *et al* 2006a, Elmendorf *et al* 2012a, 2012b, Natali *et al* 2012). Remote sensing observations and proxy data indicate widespread increases in vegetation productivity in recent decades (Forbes *et al* 2010, Beck and Goetz 2011, Guay *et al* 2014) often accompanied with an expansion of shrub cover (Myers-Smith *et al* 2011, Frost and Epstein 2014, IPCC 2014). The potential for widespread shrub expansion is of particular importance because accompanying changes in albedo (Loranty *et al* 2011) will act as a positive feedback to climate warming (Chapin *et al* 2005, Bonfils *et al* 2012). However, shrub expansion is heterogeneous in space (Tape *et al* 2012), and mounting evidence suggests that shrub responses to climate are strongest in areas with relatively high soil moisture (Elmendorf *et al* 2012b, Myers-Smith *et al* 2015, Swanson 2015) and nutrient contents (Tape *et al* 2012).

Water tracks are 5–15 m wide bands of high productivity vegetation resulting from subsurface drainage and associated increases in soil temperature, moisture, and nutrient availability driven by topography and variability in active layer depth (Chapin *et al* 1988, Hastings *et al* 1989). Water tracks contain many of the conditions thought to be necessary for shrub expansion, and have been identified as a component of the landscape capable of supporting tall shrub cover (Swanson 2015). Several studies have examined the carbon (C) cycle effects of water tracks and upslope water additions, finding increased rates of primary production and ecosystem respiration (ER) that indicate water tracks may be important for understanding the tundra C balance at landscape and regional scales (Chapin *et al* 1988, Oberbauer *et al* 1991, 1989).

Despite the known effects of water tracks on vegetation composition, C and nutrient cycling, and their likely importance for shrub expansion, they have only been mapped across a limited region on Alaska's North Slope (Walker and Maier 2007) and their distribution across Siberian landscapes remains unknown. Quantifying the areal extent of water tracks will help improve our understanding of landscape scale variability in the drivers of shrub expansion and C cycling in tundra ecosystems. This will be especially important given recent findings indicating that tall shrub distribution is limited by environmental factors, including soil wetness and thaw depth, and that tall shrubs grow along water tracks (Swanson 2015). Moreover, climate induced changes in arctic precipitation patterns (ACIA 2005, IPCC 2014) may lead to divergent ecosystem C cycle responses in these areas of complex terrain (e.g. Riveros-Iregui *et al* 2012). As a result, the goals of this study were to quantify the areal extent of water tracks and associated variability in vegetation biomass and C flux in a northeast Siberian tundra landscape. To achieve these objectives we used geospatial data to investigate water track distribution, field observations to assess environmental conditions and ecosystem-scale C flux patterns, and a simple ecosystem model alongside leaf area derived from remotely sensed data to assess landscape-scale patterns in C fluxes.

2. Materials and methods

2.1. Site description

The study was conducted in northeastern Siberia in the Sakha Republic, Russia, along the eastern bank of the Kolyma River (figure 1). Field observations were collected at Krutaya Drisva (69.34°N, 161.51°E), approximately 32 km south of the river's mouth at the Arctic Ocean, approximately 30 m above sea level, on a 2.5% northwest-facing slope. Average recorded January, July, and annual temperature and annual precipitation at the Ambarchik Bay meteorological observatory ~40 km from the site are −29.1 ± 4.1 °C, 7.6 ± 2.2 °C, −11.7 ± 2.4 °C, and 153 ± 75.0 mm, respectively, from 1950 to 2009 (Global Historical Climatology Network: http://ncdc.noaa.gov/ghcnm/v3.php). The mean temperature during the field study period from 9 July and 18 July 2014 was 14.6 °C, and mean relative humidity was 77.7%. The site contained tussock tundra and a water track (figure 2). This area is part of a region of tundra with rolling topography—which contributes to increased drainage—down slope from a nearby mountain range. The tundra within the site contained a mix of shrubs (*Betula nana* and *Salix* spp.), tussock forming sedge (*Eriophorum vaginatum*) and other sedge vegetation (*Carex* spp). The water track matched the description of Chapin *et al* (1988) and was dominated by large patches of *B. nana* and *Salix* spp. alternating with equally large patches of *Carex* spp.

2.2. Geospatial datasets

Geospatial analysis was carried out using one composite raster image and a digital surface model (DSM). These data were acquired from the Polar Geospatial Center (PGC) at the University of Minnesota. The image was orthorectified and corrected to top-atmosphere reflectance by the PGC. This data encompassed areas of tundra and boreal forest along the eastern bank of the Kolyma River, including the study site at Krutaya Drisva. The image was captured by WorldView 2 on 15th August 2011 and covers approximately 1165 km^2. It consists of eight spectral bands: RED (630–690 nm), red edge (705–745 nm), coastal blue (coastal: 400–450 nm), blue (450–510 nm), green (510–580 nm), yellow (585–628 nm), near infrared 1 (NIR1: 770–895 nm) and near infrared 2 (NIR2: 860–1040 nm) with 1.85 m nadir resolution. The DSM was generated from stereo-pairs of high-resolution imagery and covered approximately 3000 km^2 of the region. It contained a single band showing elevation at 2 m resolution with a vertical resolution of <1 m not accounting for variations in vegetation canopy height. The only other peak growing season image available from the region was a QuickBird image mosaic acquired 4–11 July 2011.

The scope of our geospatial analysis was limited to the area of these images that encompassed tundra. We considered tundra to be high latitude locations with low growing vegetation and a lack of trees (Walker *et al* 2005). Tree line was determined by eye and a polygon encompassing the 'tundra' was digitized manually. This polygon was then used to clip an area of approximately 448 km^2 from the raster files for use in geospatial analysis.

2.3. Water track mapping

A number of potential methods exist for automatically classifying water tracks and surrounding tundra including supervised, unsupervised and object oriented spectral classifications as well as topographic

analysis including flow path mapping. Given that water tracks are visible to the naked eye in high-resolution imagery, manual digitization would be the most effective means of classifying this data. However manual digitization is less feasible on a large scale and a spectral classification approach was chosen. In order to determine the best method for generating the final map of water tracks a variety of different techniques mentioned above were used to classify a small sample image—approximately 32 km^2. These classifications were compared to a map of water tracks outlined using heads up digitizing. Maximum likelihood supervised classification of all the bands present in the WorldView 2 image was deemed the best approach and was thus used in the final analysis followed by use of the boundary clean tool in ArcMap.

The entire data set was then classified and water track area was calculated (see figure 3 for overview). Training points were selected in water tracks, inter-track tussock tundra, inter-track shrub tundra and a variety of other landforms for a total of 15 training samples. These classifications were then aggregated into the broad categories of water track and inter track tundra using the reclassify tool. The normalized difference vegetation index (NDVI) was calculated on a per cell basis from the image using the equation below (equation (1))

$$\sum \frac{(\mathrm{NIR2} - \mathrm{RED})}{(\mathrm{NIR2} + \mathrm{RED})} = \mathrm{NDVI}. \quad (1)$$

NDVI compares red and near infrared radiation reflected, which can be used to determine the presence and photosynthetic capacity of vegetation (Tucker 1979). As an indicator of photosynthetic capacity NDVI is inherently tied to leaf area and gross primary production (GPP) (Williams *et al* 2006, Street *et al* 2007).

Surface water was mapped using a supervised classification and the normalized difference water index (NDWI) (equation (2))

$$\sum \frac{(\mathrm{Coastal} - \mathrm{NIR2})}{(\mathrm{Coastal} + \mathrm{NIR2})} = \mathrm{NDWI}. \quad (2)$$

NDWI compares costal blue and NIR2 to detect the presence of standing water in areas greater than a single pixel (Wolf 2012). Representative areas of surface water and tundra were selected from within the World View 2 image and a supervised classification was run using these points.

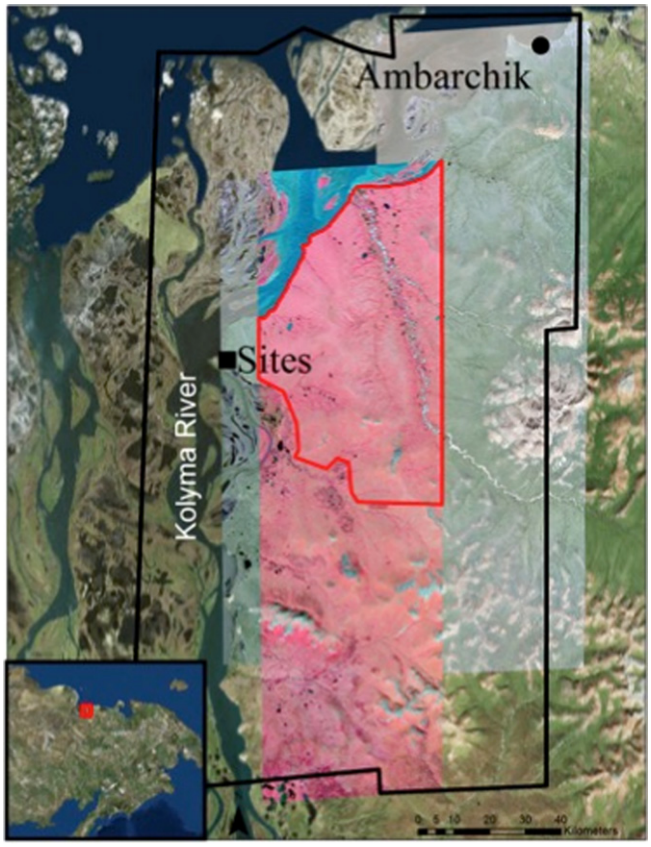

Figure 1. Map showing the study sites, the Ambarchik Bay meteorological Station, study sites, the World View 2 image in false infrared, a Quick Bird image in RGB, the extent of the DSM in black and the extent of the study area in red with the southernmost boundary representing tree line. Basemap source Esri, Copyright© Esri. All rights reserved.

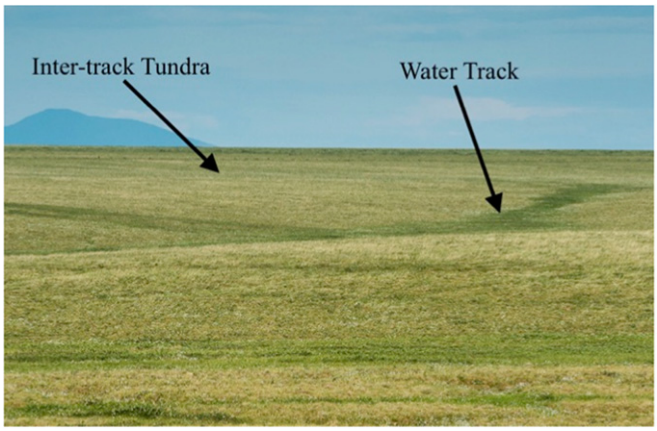

Figure 2. Photo from near the study site showing water tracks and surrounding inter-track tundra. Photo credit: Chris Linder, Copyright © Chris Linder Photography 2014.

The total area of water tracks, tundra and standing water in the study area was then calculated. The zonal statistics tool in ArcGIS and the maps produced above were used to calculate the average of leaf areas indices (LAI) and NDVI for water tracks and tundra in the entire World View 2 image.

The accuracy of our classification was assessed using 500 m diameter buffers around fifteen points randomly generated across the study area. In each location well-developed water tracks (Walker and Maier 2007) were hand digitized using the World View 2 image. The output of the supervised classification was then compared to these hand digitized samples. Our initial classification was tailored to avoid errors of commission at the expense of increased omission.

2.4. Landscape-scale CO_2 flux modeling

In order to quantify the effects of water tracks on landscape-scale CO_2 dynamics we used the model of tundra net ecosystem CO_2 exchange (NEE) developed by Shaver *et al* (2007). We chose this modeling approach because it enabled a more robust assessment of water track CO_2 fluxes by covering a wider range of vegetation and environmental conditions than would have been possible using field observations alone (described below). The model relies on the principle of functional convergence of NEE, which means that a single parameterization of an NEE model applies across all tundra plant functional types. The model requires LAI, air temperature (airT), and incident photosynthetically active radiation (I) as inputs, and has been successfully applied for numerous tundra vegetation types at a range of spatial and temporal scales (Shaver *et al* 2007, Ratstetter *et al* 2010, Loranty *et al* 2011, Stoy *et al* 2013, Sweet *et al* 2015).

The World View 2 NDVI map described above was used to produce a map of LAI with the equation and constants described by Street *et al* (2007) (equations (1) and (3)). We used the parameterization covering all vegetation types, as we did not have data detailing the distribution of individual vegetation communities (Street *et al* 2007)

$$\mathrm{LAI} = 0.0148 * e^{6.192*\mathrm{NDVI}}. \quad (3)$$

We then combined this map of LAI with 434 records of half hourly meteorological data (described below) in order to model NEE, GPP, and ER using the Raster package (Hijmans and van Etten 2012) in R (R Development Core Team 2015). NEE was modeled as in Shaver *et al* (2013, 2007) (equations (4)–(6))

$$\mathrm{NEE} = \mathrm{GPP} - \mathrm{ER}, \quad (4)$$

$$\mathrm{GPP} = \frac{P_{\mathrm{maxL}}}{k} * \ln \frac{P_{\mathrm{maxL}} + E_0 * I}{P_{\mathrm{maxL}} + E_0 * I * e^{-k*\mathrm{LAI}}}, \quad (5)$$

$$\mathrm{ER} = (R_0 * E^{\beta+\mathrm{airT}} * \mathrm{LAI}) + R_x. \quad (6)$$

We parameterized the model using the pan-Arctic parameterization from Shaver *et al* (2007, 2013): the light-saturated photosynthetic rate per unit leaf area or P_{maxL} (14.747 μmol m^{-2} leaf s^{-1}); the Beer's law extinction coefficient or k (0.5 m^{-2} ground m^{-2} leaf area); the initial slope of the light response curve or E_0 (0.041 μmol CO_2 fixed μmol^{-1} photons absorbed); the basal respiration rate or R_0 (1.177 μmol CO_2 m^2 leaf s^{-1}); the constant β (0.046 $°C^{-1}$); and a constant representing respiration in deep soil horizons or R_x (0.803 μmol CO_2). Air temperature (airT) and the top of the canopy photon flux (I) was obtained from half hourly meteorological data collected in the field, as described in the following section. Negative NEE values represent a net ecosystem sink of CO_2.

The modeling operations created 1302 raster layers at 1.84 m resolution spanning the course of the observational period. Parallel computing was implemented in R using the spatial.tool and foreach packages (Greenberg, 2014, Revolution Analytics and Weston 2014). These rasters were aggregated to calculate average GPP, NEE and ER over the ~9 day observational period. The output of the classification was combined with these to calculate average GPP, NEE and ER for inter-track tundra and water tracks.

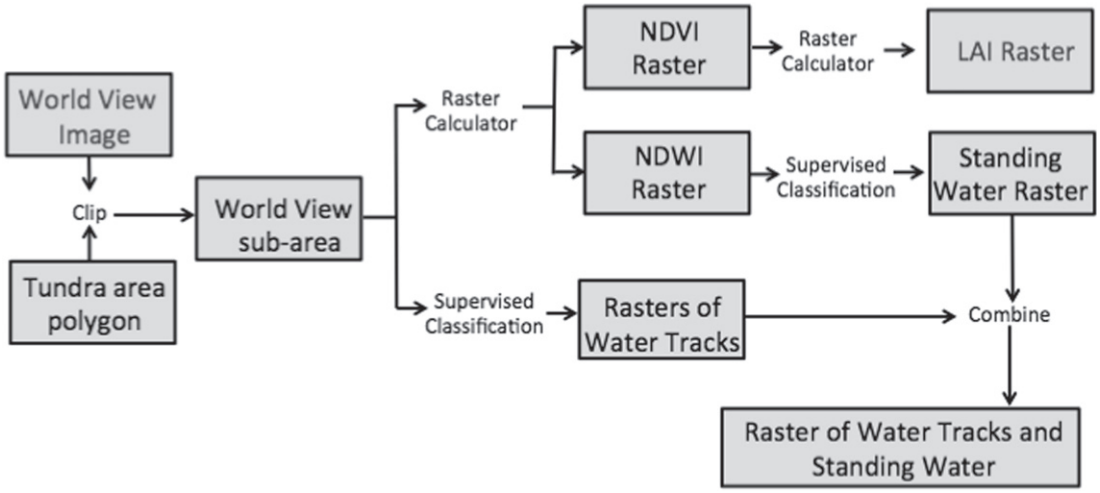

Figure 3. Process of computing final classifications and statistics.

2.5. Observations of CO_2 flux and environmental conditions

All field data were collected between 9 July and 18 July 2014. We established 12 plots inside a water track and 12 in the surrounding tundra. These 0.36 m^2 plots were spaced ~10 m apart. The tundra and water track plots were established in areas dominated by deciduous shrubs ($n = 6$) or graminoids ($n = 6$).

We measured NEE under light and dark conditions over the course of three days, resulting in a total of 84 pairs of light and dark measurements. CO_2 fluxes were measured using the static chamber technique (e.g., Shaver *et al* 2007). For each measurement a 0.3 m tall 0.36 m^2 Plexiglas chamber was placed over the ground and vegetation, and air was circulated between the chamber and a Licor infrared gas analyzer (LI840) to measure the CO_2 concentration every second for approximately 1 min. The chamber was flushed with ambient air before each measurement, and two fans inside the chamber ensured air mixing. After initial quality screening NEE and ER were calculated from light and dark fluxes respectively using the rate of change in CO_2 concentration over the measurement period (R Development Core Team 2015) and the ideal gas law (equation (1), Shaver *et al* 2007). We then calculated GPP as the difference between NEE and ER.

Each flux measurement was accompanied by measurements of soil temperature (5 cm depth), air temperature, and internal chamber temperature using a Fisher Scientific Traceable Dual-Channel Thermometer, and radiometric surface temperature using an Apogee Infrared Radiometer. Soil moisture was measured using a Decagon Devices GS3 Ruggedized Soil Moisture, Temperature and Electrical Conductivity Sensor (5 cm depth). NDVI was measured using a Decagon Devices Spectral Reflectance Sensor mounted at the end of a 1 m long PVC pipe and held approximately 1.5 m above the plot.

On three separate days, thaw depth was measured at two corners of each plot using a metal thaw depth probe. At the conclusion of the fieldwork the basal diameters of all *B. nana* and *Salix spp.* present in each plot were measured using calipers and converted to biomass using allometric equations developed for this region (Berner *et al* 2015). The environmental data from all 24 plots was averaged by plot and analyzed using both single factor and nested analysis of variance (ANOVAs) in R (R Development Core Team 2015). To compare differences between water-tracks and inter-track tundra, we grouped data by plot type (i.e. water track or inter-track tundra) across vegetation types using a single factor ANOVA. We also examined interactive effects of vegetation type (i.e. shrub or graminoid) and plot type by nesting vegetation within plot type in a nested ANOVA.

A meteorological station (Onset Corp, Bourne MA), which was located ~500 m from the water track, measured and recorded air temperature, barometric pressure, PAR, relative humidity and moisture content at the half hourly intervals from 9 July to 18 July 2014. These data were used in conjunction with measured fluxes and as model inputs.

3. Results

3.1. Distribution of water tracks

The total areas of tundra, water tracks and surface water in our study area were 408.3 km^2, 33.4 km^2 (7.4%) and 6.8 km^2, respectively (figure 4(a)). Water tracks had a mean NDVI and LAI of 0.61 and 0.65, and inter-track tundra had a mean NDVI and LAI of 0.56 and 0.47, respectively (figures 4(b) and (c)).

Our classification had overall accuracy 90.1%, user accuracy of 92.9% in inter-track tundra and user accuracy of 62.2% in water tracks (see supplemental table). Our initial classification avoided errors of commission at the expense of increased omission. This

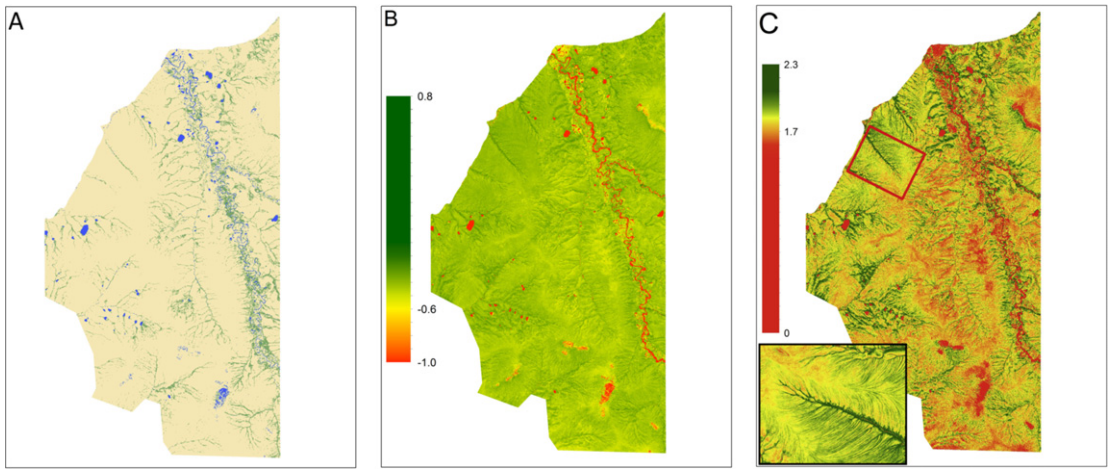

Figure 4. (a) Raster showing areas within the geospatial data classified as water track (green), tundra (tan) and surface water (blue). (b) Raster of NDVI resulting from the analysis with higher values in green. (c) Raster of LAI resulting from the analysis with higher values in green and inset view of water track.

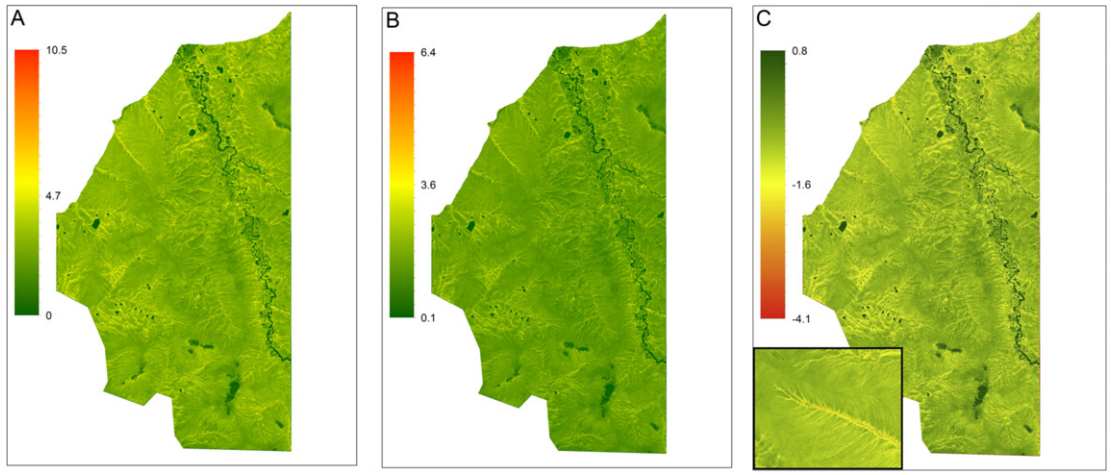

Figure 5. (a) Average modeled GPP raster with lower values in dark green. (b) Average modeled ER raster with lower values in dark green. (c) Average modeled NEE raster with lower values in dark green and inset view of water track.

conservative classification approach ensured that other tundra landforms with dense shrub cover, such as floodplains, were not falsely classified as water tracks leading to false increases in water track area, NDVI and LAI. Twenty percent of errors of commission occurred within 20 m of the digitized water track polygons suggesting that our vector digitization presented too discrete and binary a boundary between water tracks and surrounding inter track tundra leading to the omission of the fringes of water tracks and poorly developed water tracks successfully detected by the per-pixle classifier.

3.2. Field observations

Soil moisture was higher in the water tracks ($P < 0.001$) compared to inter-track tundra, and significant differences in soil moisture existed between plots of different vegetation and landform types ($P = 0.001$; table 1). Average soil temperature at 5 cm was also higher in the water track plots compared to tundra plots ($P < 0.001$; table 1); however, ground surface temperature was higher in inter-track tundra compared to water track plots ($P < 0.001$; table 1). Average thaw depth was deeper inside the water track than in the surrounding tundra ($P = 0.001$; table 1). Thaw depth was also deeper in water track shrub plots compared to inter-track shrub plots, but did not differ between graminoids plots inside and outside of the water track ($P = 0.05$). NDVI was higher in water track plots when compared to inter-track tundra ($P < 0.001$; table 1) and was also higher in shrub plots of the same landform type ($P < 0.001$; table 1). This confirms the trend observed in the satellite imagery.

Total shrub biomass was significantly greater in water track shrub plots than in inter-track shrub plots ($P < 0.001$; table 2). This trend was driven by higher *B. nana* biomass in water track shrub plots ($P < 0.001$) in spite of lower *Salix* spp. biomass when

Table 1. Averages of field observations by plot type and vegetation type[a].

Type[b,c]	Composition[c]	Soil temp.[d] (°C)	Std. err.	Soil moisture (m^3/m^3)	Std. err.	Surface temp. (°C)	Std. err.	Thaw depth (cm)	Std. err.	NDVI	Std. err.
Water track		4.6***	0.2	0.78***	0.05	8.7***	0.3	40**	2	0.66***	0.01
	Graminoid	4.7	0.3	0.90**	0.01	8.8	0.4	36*	1	0.62***	0.02
	Shrub	4.5	0.3	0.65**	0.08	8.6	0.3	43*	3	0.69***	0.01
Inter-track		3.4***	0.3	0.38***	0.03	10.9***	0.4	32**	2	0.60***	0.01
	Graminoid	3.5	0.4	0.39**	0.04	11.1	0.6	36*	2	0.57***	0.01
	Shrub	3.3	0.3	0.37**	0.03	10.8	0.5	29*	2	0.62***	0.01

[a] Significance codes: <0.001 '***' 0.001 '**' 0.01 '*' 0.05 '.'

[b] Single factor ANOVA.

[c] Nested ANOVA.

[d] 5 cm depth.

Table 2. Average plot level shrub biomass derived from allometry by plot and vegetation type[a].

		Above ground biomass (gm^{-2})					
Type[b,c]	Composition[c]	Betula *nana*	Std. err.	Salix *spp.*	Std. err.	Total	Std. err.
Water Track		56.3	17.1	55.7	23.8	112.0	29.9
	Graminoid	10.9***	6.3	14.8*	7.1	25.8***	13.0
	shrub	101.6***	20.6	95.5*	42.2	198.2***	28.1
Inter-track		39.6	8.0	67.3	32.3	106.9	33.3
	Graminoid	28.9***	9.6	7.3*	3.6	36.1***	10.6
	shrub	50.4***	11.9	127.2*	56.1	177.6***	52.7

[a] Significance codes: <0.001 '***' 0.001 '**' 0.01 '*' 0.05 '.'
[b] Single factor ANOVA.
[c] Nested ANOVA.

Table 3. Average and sum of modeled landscape level CO_2 flux.

Type	GPP (μmol CO_2 m^{-2} s^{-1})	ER (μmol CO_2 m^{-2} s^{-1})	NEE[a] (μmol CO_2 m^{-2} s^{-1})
All	2.71	1.97	−0.73
Water track	3.54	2.37	−1.18
Inter-track	2.64	1.94	−0.70

[a] Negative NEE value represents net uptake of CO_2.

compared to inter-track shrub plots ($P = 0.05$; table 2). Total shrub biomass was lower in water track graminoid plots ($P < 0.001$; table 2) than in inter-track graminoid plots.

At the landscape scale, average modeled GPP and ER were higher inside the water track and NEE was more negative relative to inter-track tundra (table 3).

Average plot-level ER was significantly higher in the water track when compared to inter-track tundra ($P < 0.001$; table 4). Average plot level GPP was also higher and there was slightly more CO_2 uptake (i.e., more negative NEE) observed.

4. Discussion

Water tracks composed 33.4 km^2 or 7.4% of the 448.63 km^2 of tundra analyzed, and they were greater net sinks of CO_2 during the observation period, based on modeled results. Although differences in observed C fluxes between water track and inter-track tundra were not statistically significant, the magnitude and direction of observed differences were similar to modeled differences which encompassed a much larger range of vegetation and environmental conditions. Observations of greater soil moisture, plant biomass, thaw depth, NDVI and C uptake in water tracks relative to inter-track tundra are consistent with patterns observed in other studies and posit a mechanism for increased productivity in water tracks (Chapin *et al* 1988, Hastings *et al* 1989, Oberbauer *et al* 1991). Other authors have attributed these increases in productivity to increased N availability resulting from deeper thaw depths, warmer soil and possibly the liberation and movement of nutrients by flowing water (Chapin *et al* 1988, Hastings *et al* 1989, Oberbauer *et al* 1989, Harms and Jones 2012, Harms *et al* 2014).

4.1. Water track mapping

Water tracks constitute a large area within the study region (7.4% of the total or 7.6% if standing water is excluded). A number of methods using different combinations of bands and supervised and unsupervised classification schemes were investigated for use in classifying water tracks in this study. The classification method, which worked best in small-scale tests (maximum likelihood supervised classification of all the bands present in the WorldView 2 image followed by use of the boundary clean tool in ArcMap), was used in the final analysis and captured the greatest number of bands at the highest resolution, thus providing the most information about a given pixel. However as a result of our conservative classification approach it consistently underestimated the area of water tracks when compared to digitization by eye and is more than likely an under estimate. Twenty percent of errors of commission occurred within 20 m of the digitized water track area suggesting that our digitization may have been too discrete and failed to account for poorly-developed water tracks (e.g. Walker and Maier 2007). Judging water track presence or absence based upon a vector boundary may have lead to the omission of the fringe of water tracks or poorly developed water tracks. The classifiers pixel based approach better captures the detailed boundary between water tracks and tundra potentially leading to apparent commission.

Given that water tracks result from subsurface flow and permafrost topography, inputs of water vary across time and space, and water track formation has been observed at decadal time scales these figures of water track area may be specific to the landscape and time period investigated (Ostendorf and Reynolds 1993, Osterkamp *et al* 2009).

Differences in remotely sensed NDVI between water tracks and inter-track tundra agree well with field observations showing greater vegetation biomass

Table 4. Averages of plot level flux measurements.

Type[c]	Composition[c,d]	GPP[a] (μmol CO_2 m^{-2} s^{-1})	Std err.	ER[a] (μmol CO_2 m^{-2} s^{-1})	Std err.	NEE[a,b] (μmol CO_2 m^{-2} s^{-1})	Std err.
Water track		4.13	0.43	2.66***	0.19	−1.34	0.31
	Graminoid	4.26	0.61	2.69	0.26	−1.60	0.56
	Shrub	4.00	0.63	2.63	0.29	−1.55	0.51
Inter-track		3.18	0.39	1.63***	0.20	−1.57	0.38
	Graminoid	2.63	0.60	1.34	0.21	−0.93	0.51
	Shrub	3.72	0.48	1.92	0.33	−1.75	0.34

[a] Significance codes: <0.001 '***' 0.001 '**' 0.01 '*' 0.05 '.'

[b] Negative NEE value represents net uptake of CO_2.

[c] Single factor ANOVA.

[d] Nested ANOVA.

and productivity from this (tables 1 and 2) and previous studies (Chapin *et al* 1988, Hastings *et al* 1989, Oberbauer *et al* 1989). NDVI is heavily correlated albeit nonlinearly with vegetation biomass in arctic ecosystems (Jia *et al* 2003, 2006). These spatial patterns in NDVI are likely the result of increased thaw depth, soil temperature and soil moisture, which in turn affect vegetation structure and function in ways similar to those observed by other authors (Chapin *et al* 1988, Hastings *et al* 1989, Oberbauer *et al* 1989). Given their large area, previous observations of variations in soil C flux and differences in vegetation composition and soil conditions, water tracks are relevant to the study of landscape scale tundra C cycling and ecosystems responses to climate warming including shrub expansion (Oberbauer *et al* 1991, Swanson 2015).

4.2. Environmental conditions

Physical environmental conditions within water tracks differed from adjacent inter-track tundra in several ways. As expected, soils were wetter in the water tracks, and the wetter soils may in turn be affecting other variables (table 1). The higher thermal conductivity associated with wetter soils along with flowing subsurface water and feedbacks between shrubs, soil temperature and permafrost is likely contributing to higher soil temperatures and deeper thaw depths in water tracks—although measurements were taken prior to the period of maximum permafrost thaw and active layer temperature (Chapin *et al* 1988, Hinzman *et al* 1991, O'Donnell *et al* 2009, Blok *et al* 2010, Shiklomanov *et al* 2010, Foster 2015). Vegetation type on the other hand does not appear to be affecting soil temperature in any significant way—albeit over a short measurement period. The observed lower surface temperature in water tracks—contrary to the trend in soil temperature—is likely due to increased latent heat flux associated with increased soil moisture and increased transpiration by vegetation biomass as well as shading of the soil surface by shrubs (Jackson 1997, Sturm *et al* 2001, Shaver *et al* 2014).

Tundra ecosystems are generally nutrient limited, and increased thaw depth coupled with soil temperature and subsurface flow may directly affect nitrogen and phosphorus availability and explain many of the changes in vegetation structure observed in water tracks (table 2; Chapin *et al* 1988, Hastings *et al* 1989, Giblin *et al* 1991, Oberbauer *et al* 1991, Naito and Cairns 2011, Harms and Jones 2012, Harms *et al* 2014). Significant increase in shrub biomass and relative abundance of *B. nana* in the water tracks parallel the effects seen in nutrient addition and warming experiments (Chapin *et al* 1995) as well as observations made in water tracks by other authors (Hastings *et al* 1989). Well established graminoid-dominated areas are also in line with similar observations made in water tracks (Hastings *et al* 1989) and significant lower shrub biomass was observed in these locations suggesting that graminoids may outcompete shrubs in certain areas. These variations in biomass are driving variations in NDVI between water tracks and inter-track tundra, which are in line with the remote sensing data and the observations of other authors (tables 1 and 2; Jia *et al* 2003, 2006, Raynolds *et al* 2006).

4.3. Carbon flux

Variability in ecosystem C fluxes inferred from modeling are consistent with observed differences in NDVI and biomass (tables 1–3) and those observed in other studies (Boelman *et al* 2003, Raynolds *et al* 2006, Sweet *et al* 2015). Both modeled GPP and ER were higher leading to more negative NEE or greater net uptake of C in the water tracks relative to inter-track tundra. Increases in ER resulting from increased biomass, deeper thaw depths, and warmer soils were complemented by increases in GPP (table 3). According to the model water tracks account for 9.9% of total GPP, 9.0% of total ER and 12.1% of NEE during the middle of the growing season, slightly higher than would be expected, given their areal distribution of 7.4% of tundra land area. GPP also increased slightly in water track graminoid plots despite decreased shrub biomass.

These estimates only account for C flux during a fraction of the peak of the growing season, and so the relative contribution of water tracks to growing season or annual landscape-scale C fluxes may be different. Phenological differences in vegetation communities during early and late season could affect C fluxes integrated over the entire growing season (Zeng *et al* 2013, Sweet *et al* 2014, 2015). Differences may also exist outside of the growing season, where C fluxes are governed largely by co-variation in snow cover and soil temperature (Webb *et al* 2016). Increased snow depth resulting from topographic relief and increased shrub cover has been documented in water tracks and other shrub dominated locations (McFadden *et al* 2001, Pomeroy *et al* 2006). Despite greater snow depths the rate of snowmelt is often accelerated in shrub tundra decreasing the magnitude of these effects (Pomeroy *et al* 2006). Variations in snow depth and snow melt have the potential to impact phenology, growing season start and length and thus vegetation structure and function (Henry and Molau 1997, Walker *et al* 2006b, Wipf *et al* 2009).

Though not all differences were significant, observed fluxes show differences between water tracks and inter-track tundra similar to those observed in the modeled data. There is a significant difference in ER between water track and inter-track tundra ($P < 0.001$; table 3) and this increase in ER is offset by an increase in NEE leading to greater net uptake of C in the water track plots. Absolute values for mean fluxes differ between observed and modeled results; however, this should be expected given the limited temporal and spatial scale over which the observed fluxes were collected and variations in LAI corresponding to vegetation type resulting from the NDVI–LAI modeling parameters used. The model incorporates a much larger range of vegetation and meteorological conditions, and performs well in predicting broad trends in ecosystem CO_2 fluxes for water track and intra-track tundra that are consistent with observations.

5. Conclusion

The results presented here show that water tracks constitute a substantial area within tundra ecosystems for this landscape in northeastern Siberia. Water tracks have soil conditions capable of supporting tall shrub expansion, (Naito and Cairns 2011, Swanson 2015) and therefore knowing their spatial distribution may help to refine predictions of vegetation change in the Arctic. The proportional contribution of water tracks to landscape-level C balance is slightly higher than their areal extent. However, differences in vegetation, and moisture and nutrient availability may lead to divergent C cycle responses relative to upland tundra under continued climate warming. Thus, knowledge of water track distribution may also improved understanding of current and future spatial variability in tundra C cycling at the landscape scale. The distribution and extent of water tracks is likely controlled by a combination of topographic, permafrost driven and climatic factors. Future work is necessary to determine how the spatial extent of water tracks varies across the tundra biome.

Acknowledgments

This work was supported by the National Science foundation and the Polaris Project (# NSF-1044610). SC and ML also received support from the Colgate University Research Council. We would also like to thank S Zimov, N Zimov, J Schade, G Fiske, L Weber and the 2014 Polaris Project participants for their input during project development and assistance in the field.

References

ACIA 2005 *Arctic Climate Impact Assessment—Scientific Report* (Cambridge: Cambridge University Press)

Beck P S A and Goetz S J 2011 Satellite observations of high northern latitude vegetation productivity changes between 1982 and 2008: ecological variability and regional differences *Environ. Res. Lett.* 029501

Berner L T, Alexander H D, Loranty M M, Ganzlin P, Mack M C, Davydov S P and Goetz S J 2015 Biomass allometry for alder, dwarf birch, and willow in boreal forest and tundra ecosystems of far northeastern Siberia and north-central Alaska *For. Ecol. Manage.* **337** 110–8

Blok D, HeijMans M M, Schaepman-Strub G, Kononov A V, Maximov T C and Berendse F 2010 Shrub expansion may reduce summer permafrost thaw in Siberian tundra *Glob. Change Biol.* **16** 1296–305

Boelman N, Stieglitz M, Rueth H, Sommerkorn M, Griffin K, Shaver G R and Gamon J 2003 Response of NDVI, biomass, and ecosystem gas exchange to long-term warming and fertilization in wet sedge tundra *Oecologia* **135** 414–21

Bonfils C J W, Phillips T J, Lawrence D M, Cameron-Smith P, Riley W J and Subin Z M 2012 On the influence of shrub height and expansion on northern high latitude climate *Environ. Res. Lett.* **7** 015503

Chapin F S III *et al* 2005 Role of land-surface changes in arctic summer warming *Science* **310** 657–60

Chapin F S III, Shaver G R, Giblin A, Nadelhoffer K and Laundre J 1995 Responsis of arctic tundra to experimental and observed changes in climate *Ecology* **76** 694–711

Chapin F S III, Fetcher N, Kielland K, Everett K R and Linkins A E 1988 Productivity and nutrient cycling of Alaskan tundra: enhancement by flowing soil water *Ecology* **69** 693–702

Elmendorf S C *et al* 2012a Global assessment of experimental climate warming on tundra vegetation: heterogeneity over space and time *Ecol. Lett.* **5** 164–75

Elmendorf S C *et al* 2012b Plot-scale evidence of tundra vegetation change and links to recent summer warming *Nat. Clim. Change* **2** 453–7

Forbes B C, Fauria M M and Zetterberg P 2010 Russian Arctic warming and 'greening' are closely tracked by tundra shrub willows *Glob. Change Biol.* **16** 1542–54

Foster K 2015 Vegetation and soil controls on permafrost active layer depth beneath tall shrubs in the low Arctic tundra *Masters Thesis* Trent University

Frost G V and Epstein H E 2014 Tall shrub and tree expansion in Siberian tundra ecotones since the 1960s *Glob. Change Biol.* **20** 1264–77

Giblin A E, Nadelhoffer K J, Shaver G R, Laundre J A and McKerrow A J 1991 Biogeochemical diversity along a riverside toposequence in arctic Alaska *Ecol. Monographs* **61** 415–35

Greenberg J A 2014 Spatial.tools: R functions for working with spatial data *R Package version 1.8*

Guay K C, Beck P S A, Berner L T, Goetz S J, Baccini A and Buermann W 2014 Vegetation productivity patterns at high northern latitudes: a multi-sensor satellite data assessment *Glob. Change Biol.* **20** 3147–58

Harms T K, Abbott B W and Jones J B 2014 Thermo-erosion gullies increase nitrogen available for hydrologic export *Biogeochemistry* **117** 299–311

Harms T K and Jones J B 2012 Thaw depth determines reaction and transport of inorganic nitrogen in valley bottom permafrost soils *Glob. Change Biol.* **18** 2958–68

Hastings S J, Luchessa S A, Oechel W C and Tenhunen J D 1989 Standing biomass and production in water drainages of the foothills of the Philip Smith Mountains, Alaska *Ecography* (*Cop.*) **12** 304–11

Henry G H R and Molau U 1997 Tundra plants and climate change: the International Tundra Experiment (ITEX) *Glob. Change Biol.* **3** 1–9

Hijmans R J and van Etten J 2012 Geographic analysis and modeling with raster data *R Package version 2*

Hinzman L D, Kane D L, Gieck R E and Everett K R 1991 Hydrologic and thermal properties of the active layer in the Alaskan Arctic *Cold Reg. Sci. Technol.* **19** 95–110

IPCC 2014 *Climate Change 2014: Impacts, Adaptation, and Vulnerability Part A: Global and Sectoral Aspects Contribution of Working Group II to the Fifth Assessment Report of the Intergovernmental Panel on Climate Change* ed C B Field *et al* (Cambridge: Cambridge University Press)

Jackson R D 1997 *Evaluating Evapotranspiration at Local and Regional Scales* (*SPIE Milestone Series MS* vol 134)) pp 649–59

Jia G J, Epstein H E and Walker D A 2003 Greening of arctic Alaska, 1981–2001 *Geophys. Res. Lett.* **30** 2067

Jia G, Epstein H and Walker D A 2006 Spatial heterogeneity of tundra vegetation response to recent temperature change *Glob. Change Biol.* **12** 42–55

Loranty M M, Goetz S J, Rastetter E B, Rocha A V, Shaver G R, Humphreys E R and Lafleur P M 2011 Scaling an instantaneous model of tundra NEE to the arctic landscape *Ecosystems* **14** 76–93

McFadden J P, Liston G E, Sturm M, Pielke R A and Chapin F S III 2001 *Interactions of Shrubs and Snow in Arctic Tundra: Measurements and Models* (IAHS-AISH Publ.) pp 317–25

Myers-Smith I H *et al* 2015 Climate sensitivity of shrub growth across the tundra biome *Nat. Clim. Change* **5** 887–91

Myers-Smith I H *et al* 2011 Shrub expansion in tundra ecosystems: dynamics, impacts and research priorities *Environ. Res. Lett.* **6** 045509

Natali S M, Schuur E A G and Rubin R L 2012 Increased plant productivity in Alaskan tundra as a result of experimental warming of soil and permafrost *J. Ecol.* **100** 488–98

Naito A T and Cairns D M 2011 Relationships between arctic shrub dynamics and topographically derived hydrologic characteristics *Environ. Res. Lett.* **6** 045506

O'Donnell J A, Romanovsky V E, Harden J W and McGuire A D 2009 The effect of moisture content on the thermal conductivity of moss and organic soil horizons from black spruce ecosystems in interior Alaska *Soil Sci.* **174** 646–51

Oberbauer S F, Hastings S J, Beyers J L and Oechel W C 1989 Comparative effects of downslope water and nutrient movement on plant nutrition, photosynthesis, and growth in Alaskan tundra *Holarct. Ecol.* **12** 324–34

Oberbauer S F, Tenhunen J D and Reynolds J F 1991 Environmental effects on CO_2 efflux from water track and tussock tundra in Arctic Alaska, USA *Arct. Alp. Res.* **23** 162–9

Ostendorf B and Reynolds J F 1993 Relationships between a terrain-based hydrologic model and patch-scale vegetation patterns in an arctic tundra landscape *Landsc. Ecol.* **8** 229–37

Osterkamp T, Jorgenson M T, Schuur E A, Shur Y L, Kanevskiy M Z, Vogel J G and Tumskoy V E 2009 Physical and ecological changes associated with warming permafrost and thermokarst in interior Alaska *Permafrost Periglacial Process.* **20** 235–56

Pomeroy J W, Bewley D S, Essery R L H, Hedstrom N R, Link T, Granger R J, Sicart J E, Ellis C R and Janowicz J R 2006 Shrub tundra snowmelt *Hydrol. Process.* **20** 923–41

Rastetter E B *et al* 2010 Processing arctic eddy-flux data using a simple carbon-exchange model embedded in the ensemble Kalman filter *Ecol. Appl.* **20** 1285–301

Raynolds M, Walker D and Maier H 2006 NDVI patterns and phytomass distribution in the circumpolar Arctic *Remote Sens. Environ.* **102** 271–81

R Development Core Team R 2015 R: a language and environment for statistical computing *R Found. Stat. Comput.* (doi:10.1007/978-3-540-74686-7)

Revolution Analytics and Weston S 2014 doParallel: Foreach parallel adaptor for the parallel package *R Package version 1.8*

Riveros-Iregui D A, Mcglynn B L, Emanuel R E and Epstein H E 2012 Complex terrain leads to bidirectional responses of soil respiration to inter-annual water availability *Glob. Change Biol.* **18** 749–56

Shaver G R, Laundre J A, Bret-Harte M S, Chapin III F S, Mercado-Díaz J A, Giblin A E, Gough L, Gould W A, Hobbie S E, Kling G W and Mack M C 2014 Terrestrial ecosystems at Toolik Lake, Alaska *Alaska's Changing Arctic: Ecological Consequences for Tundra, Streams and Lakes* (Oxford: Oxford University Press) pp 90–142

Shaver G R, Rastetter E B, Salmon V, Street L E, van de Weg M J, Rocha A, van Wijk M T and Williams M 2013 Pan-Arctic modelling of net ecosystem exchange of CO_2 *Phil. Trans. R. Soc.* B **368** 20120485

Shaver G R, Street L E, Rastetter E B, Van Wijk M T and Williams M 2007 Functional convergence in regulation of net CO_2 flux in heterogeneous tundra landscapes in Alaska and Sweden *J. Ecol.* **95** 802–17

Shiklomanov N I, Streletskiy D A, Nelson F E, Hollister R D, Romanovsky V E, Tweedie C E, Bockheim J G and Brown J 2010 Decadal variations of active-layer thickness in moisture-controlled landscapes, Barrow, Alaska *J. Geophys. Res.* **115** G00I04

Stoy P, Williams M, Evans J, Prieto-Blanco A, Disney M, Hill T, Ward H, Wade T and Street L 2013 Upscaling tundra CO_2 exchange from chamber to eddy covariance tower *Arctic Antarctarctic Alpine Res.* **45** 275–84

Street L E, Shaver G R, Williams M and Van Wijk M T 2007 What is the relationship between changes in canopy leaf area and changes in photosynthetic CO_2 flux in arctic ecosystems? *J. Ecol.* **95** 139–50

Sturm M, Racine C and Tape K 2001 Climate change: increasing shrub abundance in the Arctic *Nature* **411** 546–7

Swanson D K 2015 Environmental Limits of Tall Shrubs in Alaska's Arctic National Parks *PLoS One* **10** e0138387

Sweet S K, Gough L, Griffin K L and Boelman N T 2014 Tall deciduous shrubs offset delayed start of growing season through rapid leaf development in the Alaskan Arctic Tundra *Arctic Antarctic Alpine Res.* **46** 682–97

Sweet S K, Griffin K L, Steltzer H, Gough L and Boelman N T 2015 Greater deciduous shrub abundance extends tundra peak season and increases modeled net CO_2 uptake *Glob. Change Biol.* **21** 2394–409

Tape K D, Hallinger M, Welker J M and Ruess R W 2012 Landscape heterogeneity of shrub expansion in Arctic Alaska *Ecosystems* **15** 711–24

Tucker C 1979 Red and photographic infrared linear combinations for monitoring vegetation *Remote Sens. Environ.* **8** 127–50

Walker D A *et al* 2005 The circumpolar Arctic vegetation map the circumpolar Arctic vegetation map *J. Veg. Sci.* **16** 267–82

Walker D A and Maier H A 2007 Geobotanical maps in the vicinity of the Toolik Lake Field Station, Alaska *Biological Papers of the University of Alaska* No. 27 Institute of Arctic Biology

Walker M D, Wahren C, Hollister R D, Henry G H, Ahlquist L E, Altalog J M and Bret-Harte S M , Wookey P A 2006a Plant community responses to experimental warming across the tundra biome *Proc. Natl Acad. Sci. USA* **103** 1342–6

Walker M D *et al* 2006b Long-term experimental manipulation of winter snow regime and summer temperature in arctic and alpine tundra *Hydrol. Process.* **13** 923–41

Webb E E, Schuur E A, Natali S M, Oken K L, Bracho B, Krapek J P, Risk D and Nickerson N R 2016 Increased wintertime CO_2 loss as a result of sustained tundra warming *J. Geophys. Res. Biogeosci.* **121** 249–65

Williams M, Street L E, Van Wijk M T and Shaver G R 2006 Identifying differences in carbon exchange among arctic ecosystem types *Ecosystems* **9** 288–304

Wipf S, Stoeckli V and Bebi P 2009 Winter climate change in alpine tundra: plant responses to changes in snow depth and snowmelt timing *Clim. Change* **94** 105–21

Wolf A F 2012 Using WorldView-2 Vis-NIR multispectral imagery to support land mapping and feature extraction using normalized difference index ratios *Proc. SPIE* **8390** 83900N

Zeng H, Jia G and Forbes B 2013 Shifts in Arctic phenology in response to climate and anthropogenic factors as detected from multiple satellite time series *Environ. Res. Lett.* **8** 035036